

# Journal of Materials Chemistry A

Accepted Manuscript



This is an *Accepted Manuscript*, which has been through the Royal Society of Chemistry peer review process and has been accepted for publication.

*Accepted Manuscripts* are published online shortly after acceptance, before technical editing, formatting and proof reading. Using this free service, authors can make their results available to the community, in citable form, before we publish the edited article. We will replace this *Accepted Manuscript* with the edited and formatted *Advance Article* as soon as it is available.

You can find more information about *Accepted Manuscripts* in the [Information for Authors](#).

Please note that technical editing may introduce minor changes to the text and/or graphics, which may alter content. The journal's standard [Terms & Conditions](#) and the [Ethical guidelines](#) still apply. In no event shall the Royal Society of Chemistry be held responsible for any errors or omissions in this *Accepted Manuscript* or any consequences arising from the use of any information it contains.

## Titanium Nitride Coating to Enhance the Performance of Silicon Nanoparticles as a Lithium-Ion Battery Anode

Cite this: DOI: 10.1039/x0xx00000x

Received 00th January 2012,  
Accepted 00th January 2012

Duihai Tang, Ran Yi, Mikhail L. Gordin, Michael Melnyk, Fang Dai, Shuru Chen, Jiangxuan Song and Donghai Wang\*

DOI: 10.1039/x0xx00000x

www.rsc.org/

**Titanium nitride (TiN) coated silicon nanoparticles were synthesized via the reduction of TiO<sub>2</sub>-coated silicon nanoparticles in Nitrogen. When evaluated as an anode for lithium-ion batteries, the material exhibited stable performance and excellent coulombic efficiency for 100 charge/discharge cycles at 0.1 C rate, in addition to the significantly enhanced rate performance.**

Silicon is considered a promising high-energy anode material for lithium-ion batteries (LIBs) because of its abundance and high theoretical capacity.<sup>1,2</sup> However, its large volume change upon lithiation/delithiation can cause pulverization of Si particles, leading to loss of electrical contact.<sup>3</sup> This can result in fast capacity fading. Furthermore, the volume change can break the solid electrolyte interphase (SEI) layer formed on the Si surface.<sup>4</sup> This continually re-exposes the fresh silicon surface to the electrolyte and prompts further SEI formation, resulting in increased impedance, low efficiency, and capacity fading.<sup>5,6</sup>

Coating a protective layer on the Si surface is a widely used approach to improve the cycling stability of the silicon anodes.<sup>7,8</sup> Carbon-based materials,<sup>9,10</sup> metal particles,<sup>11,12</sup> metal oxide particles,<sup>13,14</sup> and conductive polymers<sup>15,16</sup> have been used as coating materials. Conductive coatings such as carbon, metal, and conductive polymers enhance the electrical conductivity and also physically confine the volume change, enabling silicon anodes to maintain good electrical contact and limiting pulverization during cycling.<sup>17</sup> The surface-coating layer can also act as a volumetric expansion buffer, and the incorporation of buffer materials is advantageous as they reduce volumetric expansion and fracture during cycling.<sup>18</sup> Non-conductive coating layers such as metal

oxides can function as an artificial SEI to prevent side reactions between Si and electrolyte, improving the cycling stability.<sup>19</sup>

Herein, we demonstrate that titanium nitride coating can enhance the cycling stability of silicon nanoparticle anodes. Titanium nitride (TiN), a highly-conductive material,<sup>20,21</sup> has recently been reported as a coating for anode materials in LIBs.<sup>22,23</sup> TiN coating has been used to improve the rate capability of Li<sub>4</sub>Ti<sub>5</sub>O<sub>12</sub> anodes fabricated by a gas-phase coating technique and a composite of Si/TiN formed by ball milling has been shown to have good cycling stability.<sup>24,25</sup> However, the fraction TiN, an electrochemically inactive component, is quite high in the Si/TiN composite anode. We have developed a solution approach to synthesize silicon nanoparticles with a TiN coating layer and demonstrated enhanced cycling performance using this technique. As illustrated in Fig. 1a, a TiO<sub>2</sub> layer was first coated on the surface of Si nanoparticles in solution, and subsequent thermal annealing in nitrogen led to the formation of titanium nitride coated Si particles. The titanium nitride coating enhances the electrical conductivity of the silicon nanoparticles and also provides a stable SEI layer during cycling. The Si@TiN composite anode material delivers excellent cycling stability with a high reversible specific capacity (1900 mAh/g) within 100 cycles at 0.1 C rate, in addition to the significantly enhanced rate performance (400 mAh/g at 2 C rate).

The representative synthetic procedure of the Si@TiN composite is illustrated in Fig. 1a. Commercially available silicon nanoparticles (~50 nm, 98%, Alfa Aesar), titanium tetrabutoxide (TBOT, Alfa Aesar), acetonitrile (Sigma-Aldrich), and ammonia (Sigma-Aldrich) were used without further purification. Ethanol was dehydrated by molecule sieves. The coating reaction was conducted in a mixed solvent of ethanol and acetonitrile at room temperature by

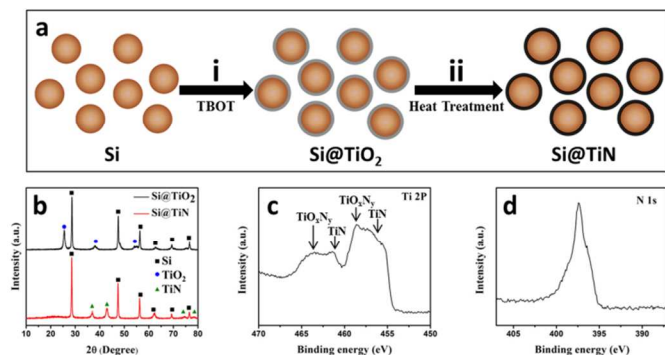


**Fig. 1.** (a) Schematic illustration of the synthesis route of Si@TiN. (b) XRD patterns of Si@TiO<sub>2</sub> and Si@TiN, (c) XPS spectra of Ti 2p in Si@TiN and (d) XPS spectra of N 1s in Si@TiN.

hydrolyzing TBOT in the presence of ammonia. In a typical experiment, 0.12 g of silicon nanoparticles were dispersed in 10 mL of ethanol/acetonitrile (3:1 v/v) and then mixed with 0.4 mL of ammonia at room temperature. Finally, a solution of 0.3 mL TBOT in 10 mL of ethanol/acetonitrile (3:1 v/v) was added to the above suspension under stirring. After reacting for 1 h, the composite was separated and collected by centrifugation, followed by washing 3 times with deionized water and ethanol, to obtain as-prepared TiO<sub>2</sub>-coated silicon powder. The powder was dried at 80 °C under vacuum for 12 h. The TiO<sub>2</sub>-coated silicon particles were thermally annealed in a tube furnace at 450 °C for 3 h, and then at 1000 °C for a further 3 h, under flowing nitrogen to make TiN-coated silicon nanoparticles. The TiO<sub>2</sub>-coated silicon nanoparticles and TiN-coated silicon nanoparticles were named Si@TiO<sub>2</sub> and Si@TiN, respectively. The obtained samples were characterized on a Rigaku Dmax-2000 X-ray powder diffractometer (XRD) with Cu K $\alpha$  radiation ( $\lambda = 1.5418 \text{ \AA}$ ). The operating voltage and current were kept at 40 kV and 30 mA, respectively. The morphologies of the products were determined using a JEOL-1200 transmission electron microscope (TEM). Chemical characterization was conducted using scanning transmission electron microscopy with an EDX accessory (STEM-EDX, Hitachi, HD-2700) and X-ray photoelectron spectroscopy (XPS, Kratos Analytical Axis Ultra). Electrochemical measurements were performed using CR2016 coin-type cells at room temperature. Slurries were prepared containing the active materials (Si, Si@TiO<sub>2</sub>, or Si@TiN), Super-P carbon, and sodium-carboxymethyl cellulose (Na-CMC) in a 6:2:2 ratio, with the Na-CMC as a 1 wt.% solution in deionized water. The viscous slurries were cast onto copper foil using a doctor-blade coating method, and then dried at 80 °C under vacuum overnight. For half-cell tests, circular working electrodes with a diameter of 12.7 mm were assembled in CR2016 coin-type cells with lithium metal as the counter electrodes and Celgard 2400 membranes as the separators in an Ar-filled glove box. 1 mol L<sup>-1</sup> LiPF<sub>6</sub> in a mixture of ethylene carbonate (EC), diethyl carbonate (DEC) and dimethyl carbonate (DMC) (1: 1: 1 v/v) and fluoroethylene carbonate (FEC, 10 vol.%) was used as the electrolyte (Novolyte Technologies, Independence, OH). The galvanostatic charge and discharge tests were carried out at rates of 0.1 C - 2 C (1 C = 4000 mA/g) between 0.01 V and 1.50 V using a battery tester (BTS-5V1mA, Neware) at room temperature. Charge/discharge rate and specific capacity were calculated based on the mass of Si, Si@TiO<sub>2</sub>, or Si@TiN materials. Electrochemical impedance spectra (EIS) of the electrodes were collected by a CHI-660 workstation, using an alternating current with amplitude of 10 mV in the frequency range of 0.1 Hz-100 kHz.

The crystallinity and phase of Si@TiO<sub>2</sub> and Si@TiN were examined by XRD. As shown in Fig. 1b, the XRD pattern of

Si@TiO<sub>2</sub> annealed at 450 °C shows peaks corresponding to crystalline silicon and anatase TiO<sub>2</sub>. When the annealing temperature is increased to 1000 °C, peaks associated with TiO<sub>2</sub> disappear while new peaks are observed at 37°, 43°, 75°, and 78°, corresponding to the (111), (200), (311), and (222) planes of titanium nitride, respectively.<sup>25</sup> The surface state of Ti and N in Si@TiN was investigated by X-ray photoelectron spectroscopy (XPS) to reconfirm the formation of TiN. As shown in Fig. 1c, in the outermost shell regions, the peaks appearing at 458.5 and 464.3 eV correspond to the Ti 2p of TiO<sub>x</sub>N<sub>y</sub>, while the peaks appearing at 455.3 and 460.8 eV correspond to the Ti 2p of TiN.<sup>26</sup> There is a small amount of TiO<sub>x</sub>N<sub>y</sub> impurities in this sample, formation of the TiO<sub>x</sub>N<sub>y</sub> phase is inevitable during sample handling.<sup>27,28</sup> As shown in Fig. 1d, the N 1s spectrum exhibits a peak at 397.0 eV, which corresponds to the N-Ti bonds.<sup>29</sup>

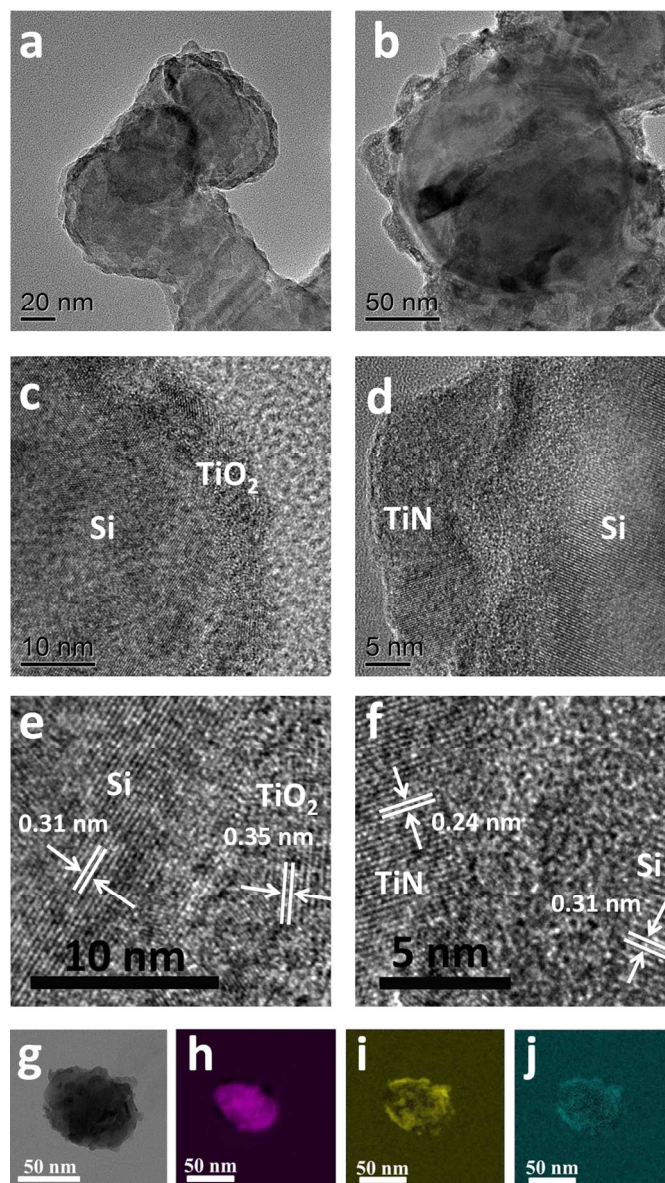


**Fig. 2.** TEM images of (a) Si@TiO<sub>2</sub> and (b) Si@TiN, HRTEM images of (c and e) Si@TiO<sub>2</sub> and (d and f) Si@TiN, and (g) a TEM image of a Si@TiN nanoparticle with corresponding EDS elemental mappings of (h) Si, (i) Ti, and (j) N for Si@TiN.

TEM investigation shows the morphology of Si@TiO<sub>2</sub> and Si@TiN. As shown in Fig. 2a and Fig. 2c, Si nanoparticles in Si@TiO<sub>2</sub> are coated with a crystalline TiO<sub>2</sub> layer composed of TiO<sub>2</sub> nanoparticles with an average particle diameter of around 10 nm. Lattice fringes of TiO<sub>2</sub> [101] with d-spacing of 0.35 nm are observed in high-resolution TEM (HRTEM) image (Fig. 2e). When the Si@TiO<sub>2</sub> was further annealed at 1000 °C in N<sub>2</sub>, the crystalline TiO<sub>2</sub> was transformed to crystalline TiN layer composed of TiN nanoparticles (Fig. 2b, and 2d, and Fig. S1 in the Supporting Information). Lattice fringes of TiN [111] with d-spacing of 0.24 nm are clearly observed in the HRTEM image (Fig. 2f) to show crystalline TiN nanoparticles coated on Si in Si@TiN. Fig. 2h-j show corresponding EDS elemental mappings of Si, Ti, and N, respectively, for the Si@TiN particle in Fig 2g. It is clear from this and Fig. 2d that the Si nanoparticles are coated with a layer composed of crystalline TiN nanoparticles. In addition, as shown in the EDS spectra in Fig. S2 in the Supporting Information, the weight percentage of silicon in the Si@TiN composite is 67.4 %.

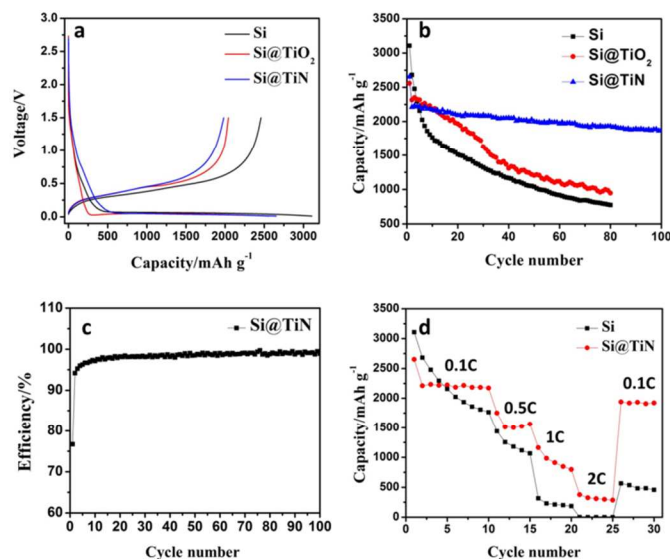


**Fig. 3.** (a) Charge and discharge curves of Si, Si@TiO<sub>2</sub>, and Si@TiN during the first cycle; (b) cycling performance of Si, Si@TiO<sub>2</sub>, and Si@TiN at 0.1 C; (c) coulombic efficiency of Si@TiN; and (d) rate capability of Si and Si@TiN.

The electrochemical performance of the Si, Si@TiO<sub>2</sub>, and Si@TiN as the anodes in LIBs was tested by galvanostatic discharging and charging at a 0.1 C rate in the potential range of 0.01 V to 1.50 V. As shown in Fig. 3a, the initial discharge and charge capacities of the Si are 3100 mAh/g and 2450 mAh/g, respectively, which correspond to an initial coulombic efficiency of 79%. The Si@TiO<sub>2</sub> composite shows initial discharge and charge capacities of 2560 mAh/g and 2040 mAh/g, respectively, with an initial coulombic efficiency of 79%. The Si@TiN composite shows initial discharge and charge capacities of 2650 mAh/g and 1990 mAh/g, respectively, with an initial coulombic efficiency of 76%. This lower efficiency is likely due to formation of some SiO<sub>2</sub> impurity in the Si@TiN composite upon annealing at 1000 °C, as has previously been shown to occur.<sup>30</sup>

The cycling performance of the Si, Si@TiO<sub>2</sub>, and Si@TiN anodes was also compared at 0.1 C rate, as shown in Fig. 3b. The Si anode shows a fast capacity fading, with discharge capacity retention of only 25% after 80 cycles. This is attributed to decreasing electrical

conductivity and formation of an unstable SEI layer. The Si@TiO<sub>2</sub> anode also shows fast capacity fading, with discharge capacity retention of 37% after 80 cycles. In contrast, the Si@TiN composite shows considerably better cyclability, with 75% capacity retention (1900 mAh/g) with respect to the first discharge capacity after 100 cycles. The rate capability of Si@TiN was compared to that of Si at rates between 0.1 C rate and 2 C rate, and is shown in Figure 3d. The Si@TiN still has a capacity of ~400 mAh/g at 2 C rate, while the Si can only achieve a low capacity of ~10 mAh/g at this rate. The enhanced rate performance of the Si@TiN is due to the TiN coating layer,<sup>25,27</sup> which can increase the conductivity of the anode.<sup>31,32</sup>

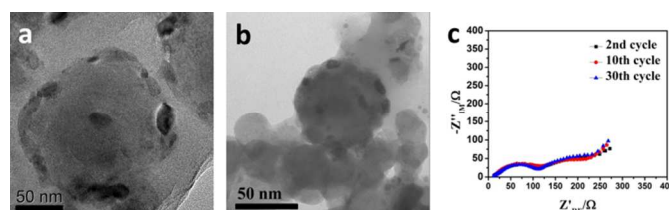


**Fig. 4.** (a) TEM image of Si@TiN after the initial discharge, (b) TEM image of Si@TiN after charge of the 30th cycle, and (c) Nyquist plots of Li-ion cells using Si@TiN electrodes for cycles at the 2nd, 10th and 30th.

As shown in Fig. 4a, the TEM image of Si@TiN after the initial discharge illustrates that the crystalline TiN nanoparticles are still on the silicon surface. To further investigate the improved cycling stability of the Si@TiN, the morphology of the material after cycling was investigated by TEM image (Fig. 4b). After 30 cycles at 0.1 C rate, the morphology of Si@TiN particles is similar to that of the pre-cycled material, and the inactive TiN layers are still anchored to the silicon surface. Electrochemical impedance spectroscopy (EIS) was also conducted on Si@TiN electrodes cycled at 0.1 C rate, as shown in Fig. 4c. The Nyquist plots of Si@TiN electrodes after 2, 10, and 30 cycles consist of two semicircles in the high-medium frequency region and a sloped line in the low frequency region. The high- and medium-frequency semicircles correspond to the SEI and interfacial charge transfer impedance, respectively, while the sloped line at low frequency is related to the diffusion of lithium ions in the electrode materials.<sup>33,34</sup> Comparison of impedance spectra from cells after 2, 10, and 30 cycles indicates that the Si@TiN electrode experiences negligible change in impedance during these 30 cycles, in contrast to increased charge transfer resistance in impedance spectra of Si and Si@TiO<sub>2</sub> anodes (Fig. S3, Supporting Information), and also suggests formation of a more stable SEI on the titanium nitride coated silicon nanoparticles than that of Si and Si@TiO<sub>2</sub>. The observation also agrees well with the stable cycling of the composite (Fig. 3b).<sup>35</sup>

## Conclusions

TiN-coated Si nanoparticles have been successfully synthesized via reduction of TiO<sub>2</sub>-coated Si. The TiO<sub>2</sub> layers were coated on the surface of silicon via a solution approach, and subsequent thermal annealing in N<sub>2</sub> led to a formation of titanium nitride coating on Si to obtain TiN-coated Si nanoparticles. The Si@TiN exhibits superior electrochemical performance as an anode for LIBs, including high specific capacity and excellent rate capability, compared with that of Si and Si@TiO<sub>2</sub> composite anodes. The enhanced performance is attributed to increased conductivity granted by the TiN coating and the more stable SEI of the Si@TiN electrode, as verified by impedance studies. This process opens up a new coating approach

for silicon-based anode materials, enabling design of new high performance lithium-ion anodes.

## Acknowledgments

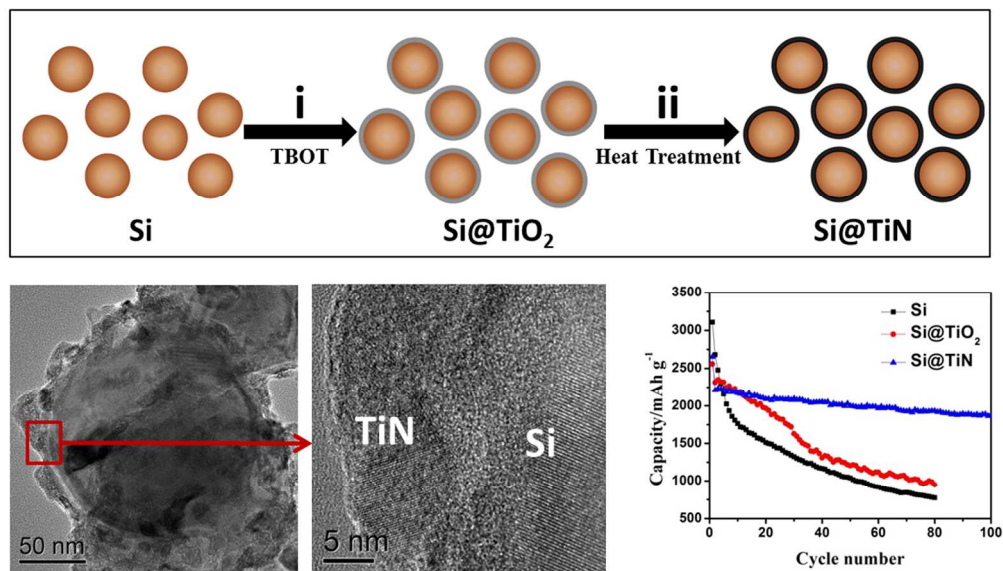
This work was supported by the Assistant Secretary for Energy Efficiency and Renewable Energy, Office of Vehicle Technologies of the U.S. Department of Energy under contract no. DE-AC02-05CH11231, subcontract no. 6951378 under the Batteries for Advanced Transportation Technologies (BATT) Program.

## Notes and references

Department of Mechanical and Nuclear Engineering, The Pennsylvania State University, University Park, Pennsylvania 16802, United States. E-mail: dwang@psu.edu; Tel: +1 814 863 1287

† Electronic Supplementary Information (ESI) available: XRD patterns, EDS spectrum, and electrochemical impedance spectra. See DOI: 10.1039/c000000x/

- 1 B. Scrosati and J. Garche, *J. Power Sources*, 2010, **195**, 2419-2430.
- 2 M. N. Obrovac and L. J. Krause, *J. Electrochem. Soc.*, 2007, **154**, A103-A108.
- 3 H. Yoo, J. I. Lee, H. Kim, J. P. Lee, J. Cho and S. Park, *Nano Lett.*, 2011, **11**, 4324-4328.
- 4 Y. C. Yen, S. C. Chao, H. C. Wu and N. L. Wu, *J. Electrochem. Soc.*, 2009, **156**, A95-A102.
- 5 R. Yi, F. Dai, M. L. Gordin, S. R. Chen and D. H. Wang, *Adv. Energy Mater.*, 2013, **3**, 295-300.
- 6 S. R. Chen, M. L. Gordin, R. Yi, G. Howlett, H. S. Sohn and D. H. Wang, *Phys. Chem. Chem. Phys.*, 2012, **14**, 12741-12745.
- 7 C. M. Ban, M. Xie, X. Sun, J. J. Jonathan, G. K. Wang, H. T. Sun, A. C. Dillon, J. Lian and S. M. George, *Nanotechnology*, 2013, **24**, 424002-424007.
- 8 S. B. Son, S. C. Kim, C. S. Kang, T. A. Yersak, Y. C. Kim, C. G. Lee, S. H. Moon, J. S. Cho, J. T. Moon, K. H. Oh and S. H. Lee, *Adv. Energy Mater.*, 2012, **2**, 1226-1231.
- 9 M. Zhou, T. W. Cai, F. Pu, H. Chen, Z. Wang, H. Y. Zhang and S. Y. Guan, *ACS Appl. Mater. Interfaces*, 2013, **5**, 3449-3455.
- 10 M. N. He, Q. Sa, G. Liu and Y. Wang, *ACS Appl. Mater. Interfaces*, 2013, **5**, 11152-11158.
- 11 J. B. Kim, H. Y. Lee, K. S. Lee, S. H. Lim and S. M. Lee, *Electrochem. Commun.*, 2003, **5**, 544-548.
- 12 S. Murugesan, J. T. Harris, B. A. Korgel and K. J. Stevenson, *Chem. Mater.*, 2012, **24**, 1306-1315.
- 13 Y. He, X. Yu, Y. Wang, H. Li and X. Huang, *Adv. Mater.*, 2011, **23**, 4938-4941.
- 14 S. H. Nguyen, J. C. Lim and J. K. Lee, *J Appl Electrochem*, 2014, **44**, 353-360.
- 15 Y. Yao, N. Liu, M. T. McDowell, M. Pasta and Y. Cui, *Energy Environ. Sci.*, 2012, **5**, 7927-7930.
- 16 Z. P. Guo, J. Z. Wang, H. K. Liu and S. X. Dou, *J. Power Sources*, 2005, **146**, 448-451.
- 17 D. N. Wang, J. L. Yang, J. Liu, X. F. Li, R. Y. Li, M. Cai, T. K. Sham and X. L. Sun, *J. Mater. Chem. A*, 2014, **2**, 2306-2312.
- 18 D. M. Piper, T. A. Yersak, S. B. Son, S. C. Kim, C. S. Kang, K. H. Oh, C. M. Ban, A. C. Dillon and S. H. Lee, *Adv. Energy Mater.*, 2013, **3**, 697-702.
- 19 J. C. Li, L. Baggetto, S. K. Martha, G. M. Veith, J. Nanda, C. D. Liang and N. J. Dudney, *Adv. Energy Mater.*, 2013, **3**, 1275-1278.
- 20 B. Y. Yuan, M. Yang and H. M. Zhu, *J. Mater. Res.*, 2009, **24**, 448-451.
- 21 Y. B. Xie, Y. Wang and H. X. Du, *Mater. Sci. Eng., B*, 2013, **178**, 1443-1451.
- 22 U. K. Bhaskara, S. Bid, B. Satpatie and S. K. Pradhand, *J. Alloys Compd.*, 2010, **493**, 192-196.
- 23 X. M. Zhao, Q. Zhou, H. Ming, J. Adkins, M. G. Liu, L. L. Su and J. W. Zheng, *Ionics*, 2013, **19**, 1843-1848.
- 24 M. Q. Snyder, S. A. Trebukhova, B. Ravdel, M. C. Wheeler, J. DiCarlo, C. P. Tripp and W. J. DeSisto, *J. Power Sources*, 2007, **165**, 379-385.
- 25 I. Kim, P. N. Kumta and G. E. Blomgren, *Electrochem. Solid-State Lett.*, 2000, **3**, 493-496.
- 26 C. H. Chen, C. E. Cheng, C. C. Hsu, M. N. Chang, H. W. Shiu and F. S. Chien, *J. Phys. D: Appl. Phys.*, 2012, **45**, 215307-215312.
- 27 M. Zukalova, J. Prochazka, Z. Bastl, J. Duchoslav, L. Rubacek, D. Havlicek and L. Kavan, *Chem. Mater.*, 2010, **22**, 4045-4055.
- 28 X. F. Wang, V. Raju, W. Luo, B. Wang, W. F. Stickle and X. L. Ji, *J. Mater. Chem. A*, 2014, **2**, 2901-2905.
- 29 L. S. Yang, H. X. Yu, L. Q. Xu, Q. Ma and Y. T. Qian, *Dalton Trans.*, 2010, **39**, 2855-2860.
- 30 B. S. Richards, J. E. Cotter and C. B. Honsberg, *Applied Physics Letters*, 2002, **80**, 1123-1125.
- 31 A. Kohandehghan, P. Kalisvaart, k. Cui, M. Kupsta, E. Memarzadeh and D. Mitlin, *J. Mater. Chem. A*, 2013, **1**, 12850-12861.
- 32 J. G. Tu, W. Wang, S. Q. Jiao, J. G. Hou, K. Huang and H. M. Zhu, *Mater. Chem. Phys.*, 2012, **136**, 863-867.
- 33 Y. M. Lin, K. C. Klavetter, P. R. Abel, N. C. Davy, J. L. Snider, A. Heller and C. B. Mullins, *Chem. Commun.*, 2012, **48**, 7268-7270.
- 34 H. C. Tao, L. Z. Fan and X. Qu, *Electrochim. Acta*, 2012, **71**, 194-200.
- 35 S. H. Park, H. K. Kim, D. J. Ahn, S. I. Lee, K. C. Roh and K. B. Kim, *Electrochem. Commun.*, 2013, **34**, 117-120.



160x92mm (300 x 300 DPI)